Journal of the Brazilian Society of Mechanical Sciences and Engineering (2023) 45:573
https://doi.org/10.1007/s40430-023-04473-7

TECHNICAL PAPER

Effect of the air flows ratio on energy behavior and NO_x emissions from a top-lit updraft biomass cookstove

Duvan F. Muñoz[1] · Jonatan Gutiérrez[1] · Juan F. Pérez[1]

Received: 7 August 2022 / Accepted: 9 September 2023

Abstract

Biomass as an energy source for three-stone cookfires is commonly used for cooking and heating rural and isolated households in developing countries; therefore, indoor air quality decreases. In this work, the effect of the air flows ratio (combustion air/gasification air, CA/GA: 2.8, 3.0, and 3.2), and the start type, cold (CS), and hot (HS), on the energy behavior and emissions from a forced-draft top-lit updraft (TLUD) cookstove, using wood pellets as fuel, is studied. Furthermore, the gasification process was thermodynamically characterized. The TLUD cookstove assessment was carried out following a modified water boiling test (WBT). The highest thermal efficiency of the cookstove was 26.74%. The lowest specific CO, NO_x, and total suspended particle matter (TSPM) emissions were 1.8 g/MJ_d, 106 mg/MJ_d, and 78.32 mg/MJ_d, respectively; this was attributed to a proper mixture between the producer gas and the combustion air. The gasification process showed a better energy yield under the hot start due to the preheating induced in the cookstove reactor. The optimal values of the producer gas heating value (LHV_{pg}), cold gas efficiency (CGE), and the biochar yield (Y_{char}) were 3.53 MJ/Nm^3, 58.61%, and 12.49%, respectively. Here, an opposite effect was found for the air flows ratios assessed. The cookstove behavior improved as the mixture between CA and GA was suitable, achieving the maximum at CA/GA = 3.0. However, the NO_x emissions increased with the increment of CA/GA ratios (from 2.8 to 3.2). Therefore, future works must address the NO_x emission reduction without penalizing performance or permanent emissions from the TLUD cookstoves.

Keywords Total suspended particle matter · Carbon monoxide · Forced draft cookstove · Wood pellets · Modified water boiling test

Abbreviations

ANOVA	Analysis of variance
CA	Combustion air
CA/GA	Combustion air/gasification air ratio
CGE	Cold gas efficiency (%)
CH_4	Methane
CO	Carbon monoxide
CO_2	Carbon dioxide
$C_{p,w}$	Water-specific heat (J/g°C)
CS	Cold start
CS.S1	Cold start stage 1
CS.S2	Cold start stage 2
$E_{e,w,bms}$	Energy to evaporate water from biomass (J)
E_{w1}	Energy delivered to water in stage 1 (J)
E_{w2}	Energy delivered to water in stage 2 (J)
F_{rg}	Biomass-air equivalence ratio [dimensionless)
GA	Gasification air
h_{fg}	Water vaporization enthalpy (J/g)
H_2	Hydrogen
HNC	Hydrogen cyanide
HS	Hot start
HS.S1	Hot start stage 1
HS.S2	Hot start stage 2
$LHV_{biochar}$	Biochar low heating value (J/g)
LHV_{bms}	Biomass low heating value (J/g)
LHV_{pg}	Producer gas heating value (MJ/Nm^3)
M	Biomass moisture content (%)
$m_{bms,c}$	Biomass consumed in wet base (g)

Technical Editor: Mario Eduardo Santos Martins.

✉ Juan F. Pérez
juanpb@udea.edu.co

Duvan F. Muñoz
duvan.munoz@udea.edu.co

[1] Group of Efficient Management of Energy (GIMEL), Department of Mechanical Engineering, Faculty of Engineering, Universidad de Antioquia, Street 67 #, 53-108 Medellín, Colombia

Published online: 09 October 2023

$m_{bms,c,d}$	Dry biomass mass consumed (g)
m_{TSPM}	Particulate matter mass (g)
$m_{w,b}$	Heated water mass (g)
$m_{w,h}$	Evaporated water mass (g)
NCE	Nominal combustion efficiency (%)
NH_3	Ammonia
NO_x	Nitrogen oxides
O_3	Ozone
PM	Particulate matter
S1	Stage 1
S2	Stage 2
SE_{CO}	Specific emission of carbon monoxide (mg/MJ_d)
SEi	Specific emission of pollutant species (mg/MJ_d)
SE_{NO}	Specific emission of nitric oxide (mg/MJ_d)
SE_{NO2}	Specific emission of nitrogen dioxide (mg/MJ_d)
SE_{TSPM}	Specific emission of total suspended particle matter (mg/MJ_d)
SO_2	Sulfur dioxide
T_{dry}	Biomass drying temperature (°C)
t_p	Total time of test duration (s)
$T_{w,i,bms}$	Biomass initial temperature (°C)
$T_{w,f}$	Final temperature of water (°C)
$T_{w,i}$	Initial temperature of water (°C)
TLUD	Top-lit updraft
TSPM	Total suspended particle matter
$\dot{V}$	Combustion gas volumetric flow (m^3/s)
$\dot{V}_{duct}$	Total volumetric flow of the gases (m^3/s)
$\dot{V}_{Vaccum\ pump}$	Vacuum pump flow (m^3/s)
WBT	Water boiling test
Y_i	Volumetric or mol fraction of gaseous species (m_i^3/ m_{gas}^3)
Y_{ijk}	Answer variables
Y_{char}	Biochar yield (%)

1 Introduction

The world's rural population is still dependent on solid fuels. About 3000 million people use biomass for cooking and heating their homes [1]. Traditional cookstoves for cooking entail high fuel consumption and pollutant emissions. Given that direct biomass combustion does not guarantee the complete oxidation of fuel, the heat released, and thermal efficiency is low (10–14%) [2]. The use of poorly efficient cookstoves is typical in the most vulnerable communities in developing countries [3], which harms the environment and the population that spend more time at home and live alongside combustion products. According to the World Health Organization (WHO), about 4.2 million people die every year due to prolonged exposition to pollutant emissions (CO, NO_x, and $PM_{2.5}$) [4]. Worldwide, during the 2001–2015 period, nitrogen oxide emissions from solid fuels (biomass) burning were determined at ~ 14.65 Tg NO_x/year [5]. The secondary formation of $PM_{2.5}$ occurs due to chemical reactions in the atmosphere of main precursors, such as NO_x, SO_2, and NH_3 [6]. Furthermore, NO_x is the precursor of ground-level ozone (O_3) formation, a primary component of photochemical smog related to airway irritation and severe asthma, among others [7, 8].

In Colombian rural communities, about 1.6 million families depend on firewood to satisfy their energy needs for cooking [9]. Aguilar-Gil et al. [10] reported that approximately 15,000 people die in Colombia every year because of air pollution; 47% from these are caused by pollution inside homes in non-interconnected zones. Therefore, it is necessary to develop efficient cooking systems focused on increasing their energy efficiency, while reducing fuel consumption and specific emissions of NO_x, CO, and $PM_{2.5}$. The optimal efficiency of the cookstove brings about a better indoor air quality where biomass is used for domestic tasks.

TLUD biomass cookstoves characterization has given rise to a higher efficiency caused by cleaner combustion and low pollutant emissions [3, 11–14]. Kirch et al. [15] compared the thermal efficiency of a forced-draft TLUD cookstove to another natural-draft TLUD stove, by using the nominal combustion efficiency (NCE). The forced-draft cookstove showed an NCE of 84.04%, while the natural-daft cookstove reached an NCE of 65.72%. The higher airflow supplied provides enough oxygen for a complete producer gas combustion and allows to obtain a higher efficiency for the forced-draft cookstove.

The air supply rate defines the gasification and combustion regimes of the biomass. The primary air determines the air/biomass ratio and solid–gas conversion velocity, whereas the secondary air oxidates the producer gas. These phenomena directly affect the cookstove efficiency and pollutant emissions (incomplete combustion increases CO and TSPM emissions). Caubel et al. [16] found that by increasing secondary airflow from 5.3 to 8.5 L/min, CO and $PM_{2.5}$ emissions decreased between 55 and 75%, while the combustion efficiency increased from 95 to 98%. The improvement in combustion also led to an enhancement in the cookstove thermal efficiency, which increased from 29 to 32%. The higher velocities of the secondary air jet provide a more turbulent mixture and oxygen in the combustion zone, favoring complete oxidation of the producer gas. Sonarkar et al. [17] noted the importance of the control of the primary (gasification-air) and secondary (combustion-air) air ratio to improve the cookstove's efficiency. The efficiency of a natural-draft TLUD cookstove was 26.5%, while the efficiency of the gasification-based cookstoves (forced-draft) was between 44.5 and 47%. Tryner et al. [18] reported an optimal CO emission of ~ 4 g/MJ and ~ 6 g/MJ with CA/GA

ratios of 3:1 for dry biomass (moisture content < 7%) and 4:1 for biomass with moisture content higher than 15%, respectively. The control in the combustion air (secondary air) and gasification air rates (primary air) favors the mixing between the air and producer gas, which contributes to keeping the flame and favoring a complete combustion.

Concerning the biomass gasification temperature in improved cookstoves, Metha et al. [19] reported an increase in the gasification temperature with the air superficial velocity because the biomass/air ratio tends toward stoichiometric ratio, which leads to an increase in the cookstove efficiency due to the higher temperature. The maximum low heating value of the producer gas (4 MJ/m^3) was reached with a primary air velocity of 0.09 m/s. Kshirsagar et al. [20] analyzed the relations between 5 controllable process variables (secondary air intake area, secondary air mass flow, pot separation, fuel surface/volume ratio, and the pot diameter) on the efficiency and emissions of an advanced cookstove. The optimal configuration of the controllable process parameters (the secondary air mass flow: 1.4 g/s and pot separation: 14 mm) led to the finding of the highest efficiency (26.5%), with CO specific emissions and a PM of 2.2 g/MJ$_d$ and 34.67 mg/MJ$_d$, respectively. This finding is attributed to a proper oxidation of the producer gas, which allows for an emission reduction and an increased efficiency.

Bhattu et al. [21] analyzed the effect of the temperature in the combustion zone and fuel type (beech wood, wood pellets, and wheat pellets) on the NO_x emissions from six improved cookstoves with different operation types (continue and batch). NO_x emissions with temperatures lower than 1100 °C were attributed to the nitrogen present in the fuel. However, NO emissions were stable regardless of the technology and were ~ 1.0 ± 0.3 g/kg of burned wood. When changing wood for wheat pellets, NO emissions increased by a factor of ~ 3.6 due to the increment in the nitrogen content of pellets. Shrestha et al. [22] measured NO_x specifically from nine Chinese gasification-based stoves (five natural drafts and four forced drafts), six of which were water-heating stoves and three were radiant-heating stoves. The average emission factor for the nine improved stoves was 336 mg/MJ, which was primarily associated with the fuel nitrogen (0.3 wt%).

Scharler et al. [23] applied a theoretical–experimental methodology seeking to improve efficiency and to reduce the CO emissions from a gasification-based cookstove (TLUD type). The assessment was carried out by linking a CFD model of gas-phase combustion with experimental results from different cookstove prototypes under water boiling tests. In the cookstove prototypes, a freeboard between the secondary air injection and the pot was modeled with different designs in order to favor the producer gas combustion. Therefore, the CO emissions diminished by 51.5%, while the efficiency reduction was mild (1.6%). Thus, although the energy characterization of the improved cookstoves and their main emissions (CO and particle matter) has been widely studied, works assessing NO_x are scarce. Therefore, this work aims to study the effect of the air flows ratio (combustion-air/gasification-air), a controllable parameter in the cookstove operation, on the energy behavior. Therefore, the thermal efficiency and specific emissions (CO, TSPM, and NO_x) of a forced-draft gasification-based (TLUD) biomass cookstove are determined following a modified WBT version 4.2.3. Furthermore, the biomass gasification process is thermodynamically characterized through the assessment of four key parameters such as cold gas efficiency (CGE), producer gas composition, producer gas heating value (LHV_{pg}), and biochar yield (Y_{char}). This thermochemical process is the cornerstone for making the most of the biomass in cooking processes in an eco-efficient way. This work aims to contribute to better understanding and developing improved gasification-based biomass cookstoves with high efficiency and low pollutant emissions.

2 Materials and methods

The effect of the combustion-air/gasification-air ratio (CA/GA: 2.8, 3.0, and 3.2) on the energy and environmental performance of a TLUD biomass cookstove was assessed. The experimental characterization is carried out by analyzing two control volumes: (1) the thermal efficiency of the cookstove under the modified WBT version 4.2.3 and (2) the thermodynamic characterization of the gasification process.

2.1 Fuel

The biomass used as fuel was wood pellets whose ultimate analysis ash-free basis is: 46.83% C, 5.67% H, 47.48% O, and 0.02% N. The carbon, nitrogen, and hydrogen were determined under the ASTM D5378-08 standard, while the oxygen was calculated by difference. The proximate analysis of the biomass evidenced a content of 84.64% for volatile matter, 14.09% of fixed carbon, 1.27% of ash, and 7.91% of moisture content. Furthermore, the biomass bulk density is 559.97 kg/m^3, with a packing factor of 0.48. The lower heating value of the pellets is 19.03 MJ/kg. The average size of the pellets ranged between 10 and 15 mm in length and 8 mm in diameter; smaller sizes tend to fluidize, which prevents reactor obstructions, and decrease the radiative heat transfer penetration in the solid phase [24]. This size favors the gasification process under stable conditions [25].

2.2 Experimental installation

Figure 1 shows the outline of the experimental setup, with its instrumentation, used to carry out the thermodynamic

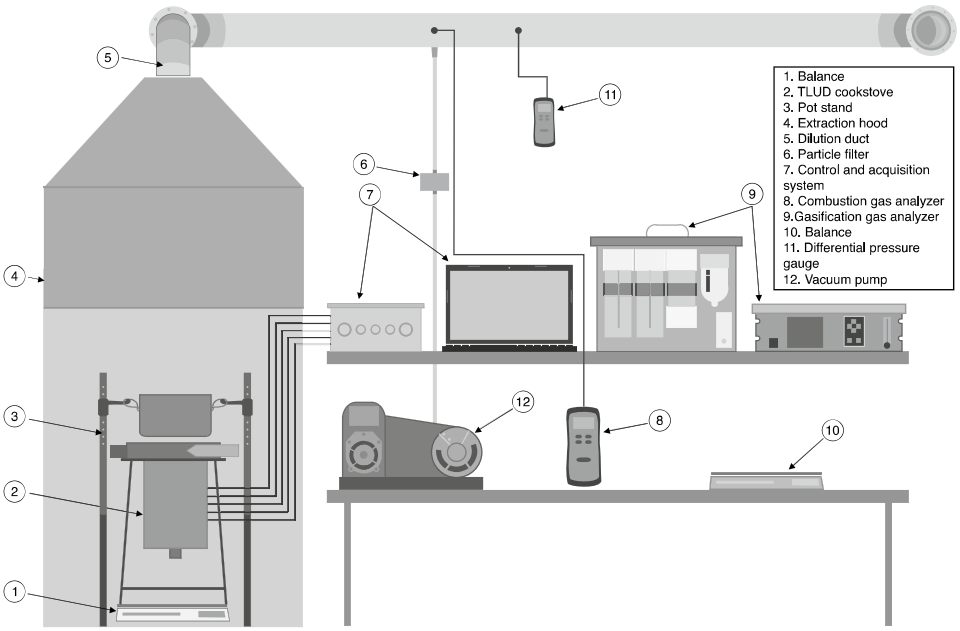

Fig. 1 Experimental setup of the biomass gasification-based cookstove

efficiency tests of the cookstove according to the modified WBT 4.2.3, as well as the thermodynamic characterization of the gasification process.

The experimental tests were carried out with ~ 1300 g of biomass in the bed (total capacity of the reactor). For the biomass ignition, 3 ml of ethanol at 95% is added to the top of the cookstove. The air required for the gasification is supplied through the lower part of the reactor body, and thus the flame front movement is opposed to the producer gas (syngas) flow (inverted downdraft reactor) [26]. The combustion air enters through the top of the stove where the combustion chamber is located to oxidize the producer gas. The energy produced by the exothermic reaction is used to boil water, while the combustion gases exit through the fume hood toward the environment.

The cookstove geometry is cylindrical with an inner diameter of 0.16 m and a height of 0.28 m. The temperature in the gasification bed was measured using 5 K-type thermocouples (± 1 °C), placed 0.04 m from each other and put inside at a depth of 5 mm into the bed to avoid the formation of air paths in the flame front and to properly develop WBT under cold and hot starts [27]. The GA was supplied through a pipe with a 0.04 m diameter, with a 12 V–0.06A axial fan, with a fixed air mass flow per cross section of 0.12 kg/m^2/s ± 3.0%, while the CA was injected into the combustion chamber with two 5V–0.14A axial fans. The combustion chamber design and dimensions are shown in Fig. 2. The experimental setup and the instrumentation used are presented in detail by Gutiérrez et al. [28].

The producer gas (syngas) composition was measured by using a Gasboard-3100 Serial (Cubic-Ruiyi Instrument) gas analyzer. The composition of combustion gases

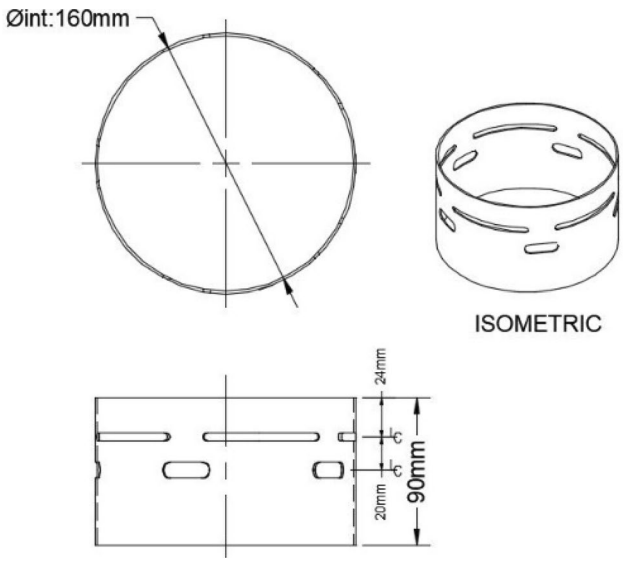

Fig. 2 Combustion chamber design of the biomass gasification-based cookstove

was measured with a KIGAZ 310 (KIMO® Instruments) gas analyzer, and a K-type thermocouple measured the gas temperature. The particulate matter (PM) collection was carried out with Advantec GC-50 glass fiber filters with a 47 mm diameter. The filters were conditioned to a temperature of 20 °C ± 3 °C with a relative humidity of 40% ± 5% during 24 h. The filters were installed into a filter holder fitted in a stainless-steel probe with 6.35 mm (1/4 in) diameter which is joined to a vacuum pump with a volumetric flow of 24 ± 0.5 L/min. To measure gas flow in the dilution duct, a Pitot tube and a Fieldpiece SDMN5 differential pressure

manometer were used for measuring the dynamic (±0.5 mmWC) and static pressures (±0.5 mmWC) [29, 30].

2.3 Modified WBT 4.2.3 protocol

The modified WBT version 4.2.3 used to characterize TLUD biomass cookstove is shown in Fig. 3. In this water boiling test, two types of starts are considered: cold start (CS) and hot start (HS). The goal is to increase the water temperature from ambient temperature (~25 °C) up to its boiling point. There are two stages for each of the starts (S1 and S2, see Fig. 3). In stage 1 of the cold start (CS.S1), 3 L of water is brought to a boiling point from ambient temperature to ~94 °C. The S1 stage starts at ambient temperature in both water and the cookstove. In stage 2 (CS.S2), the boiled water mass is weighed and put on the cookstove again. CS.S2 aims to keep boiling temperature to simulate sustained cooking, while the measured variables are recorded to determine thermal efficiency, pollutant emissions, gaseous, and total suspended particle matter (TSPM).

Once CS.S2 ends, the biochar is weighed and removed from the cookstove grate. The cookstove is loaded again with fresh biomass in order to run the hot start. The preheated cookstove is turned on and a pot with water (3 L) at room temperature is put on while ensuring that the time between the end of the cold start and the beginning of the hot start is less than 10 min [27]. Stages 1 and 2 of the hot start are named HS.S1 and HS.S2, respectively. The water heating processes under the hot start and the cold start are similar; the water is boiled from ambient temperature (25 °C). CS and HS differ in the HS.S1 because the test begins with the preheated cookstove. In stage HS.S2, water continues at boiling point under the same conditions of biomass consumption, i.e., under the fixed gasification air supplied to the cookstove. This simulates a long and controlled cooking process and, thus, gets more performance-related data such as time of stage, flue gases concentration, and TSPM.

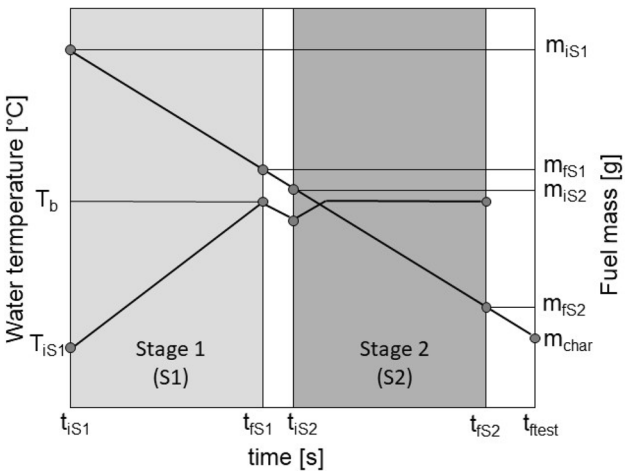

Fig. 3 Modified water boiling test (WBT) 4.2.3 protocol

2.4 Parameter calculation of the WBT protocol

The energy behavior parameters of the TLUD cookstove are calculated with data acquired during both starts (cold and hot) and their respective stages [31, 32]. The calculation of the cookstove thermal efficiency (η, %) is shown in Eq. (1).

$$\eta = \frac{m_{w,b} \cdot C_{pw} \cdot \left(T_{w,f} - T_{w,i}\right) + m_{w,h} \cdot h_{fg}}{m_{b\ ms,c,d} \cdot LHV_{bms} - m_c \cdot \mathrm{LHV}_{biochar} - E_{e,w,bms}} \cdot 100 \quad (1)$$

where $m_{w,b}$ is the heated water mass (g); $C_{p,w}$ is the water-specific heat (4.18 J/g°C); $T_{w,i}$ and $T_{w,f}$ are the initial and final temperatures of the water (°C), respectively; $m_{w,h}$ is the evaporated water mass (g), h_{fg} is the water vaporization enthalpy (2260 J/g); $m_{bms,c,d}$ is the dry biomass mass consumed (g); LHV_{bms} is the lower heating value of the biomass (J/g); m_c is the residual biochar mass at the end of the WBT protocol (g); $\mathrm{LHV}_{biochar}$ is the biochar heating value (28,800 J/g), and $E_{e,w,bms}$ is the energy associated with the vaporization of water present in the biomass (J), as presented below (Eq. (2)).

$$E_{e,w,bms} = m_{bms,c} \cdot M \cdot \left(C_{pw} \cdot \left(T_{dry} - T_{w,i,bms}\right) + h_{fg}\right) \quad (2)$$

where $m_{bms,c}$ is the biomass consumed in the wet base; M is the biomass moisture content (%); T_{dry} is the biomass drying temperature (°C); $T_{w,i,bms}$ is the biomass initial temperature ambient (°C). The specific emissions of pollutant species (SE_i), such as CO, NO, and NO_2, are calculated per unit of energy delivered to the pot in the boiling process (g/MJ_d), see Eq. (3) [33].

$$\mathrm{SE}_i = \frac{y_i \cdot \rho_i \cdot \dot{V} \cdot t_p}{E_{w1} + E_{w2}} \quad (3)$$

where y_i (i = CO, NO, and NO_2) is the volumetric or molar fraction of each gas species (m_i^3/m_{gas}^3); ρ_i is the density of each gas species (kg_i/m_i^3); $\dot{V}$ is the volumetric flow of the combustion gases (m_{gas}^3/s); t_p is the total time of the test duration (s); E_{w1} and E_{w2} correspond to the energy delivered to water throughout the WBT (MJ_d), which are calculated according to Eq. (4).

$$E_{w,i} = m_{w,b} \cdot C_{p,w} \cdot \left(T_{w,f} - T_{w,i}\right) + m_{w,h} \cdot h_{fg} \quad (4)$$

where $m_{w,b}$ is the heated water mass (g); $m_{w,h}$ is the evaporated water mass (g), and h_{fg} is the water vaporization enthalpy (2260 J/g). Otherwise, specific emissions of the total suspended particle matter (SE_{TSPM}) are calculated by Eq. (5) [34, 35].

$$SE_{\mathrm{TSPM}} = \frac{m_{\mathrm{TSPM}}}{E_{\mathrm{w},1} + E_{\mathrm{w},2}} \cdot \frac{\dot{V}_{\mathrm{duct}}}{\dot{V}_{\mathrm{vaccumpump}}} \quad (5)$$

where m_{TSPM} is the particle matter mass (mg) collected in the glass fiber filter; $\dot{V}_{\mathrm{duct}}$ is the total volumetric flow of the gas that flow through the dilution duct (m^3/s), and $\dot{V}_{\mathrm{vaccum,\ pump}}$ is the vacuum pump flow (m^3/s) [36, 37].

2.5 Characterization of the gasification process

The characterization of the gasification process was carried out for each type of start based on the modified WBT version 4.2.3. Four key parameters were calculated, such as the composition and heating value of the producer gas (LHV_{pg}) [25]. The cold gas efficiency (CGE, %) relates the energy (or power) of the producer gas with the energy (or power) supplied by the biomass in the thermodynamic process of biomass conversion into gas [38, 39]. The biochar mass yield (Y_{char}, wt%) is the residual biochar present in the bed grate once each test ends, whether under cold start or hot start. The equations proposed for calculating the parameters described above are presented in detail by Gutierrez et al. [28].

2.6 Statistical experimental design

The aim is to evaluate the significance of the factors (CA/GA ratio and start type—CS and HS) on the answer variables of the TLUD biomass cookstove. The parameters η (%), SE_{CO} (g/MJ_d), SE_{NO} (g/MJ_d), SE_{NO2} (g/MJ_d), and SE_{TSPM} (mg/MJ_d) are the answer variables assessed. The CA/GA ratio factor has 3 levels (2.8, 3.0, and 3.2), while the start factor has two levels (CS and HS). The experimental factors were assessed following the modified WBT version 4.2.3. Therefore, a 3×2 factorial experimental design was adopted, see Eq. (6). The combination of the levels of each factor produced a total of six experimental tests, plus an additional replica of the whole experimental campaign, for a total of twelve tests. Therefore, the answer variables shown in next section correspond to the average values between the experimental test and its replica.

$$Y_{ijk} = \mu + \tau_i + \beta_j + (\tau\beta)_{ij} + \varepsilon_{ijn} \quad (6)$$

where μ is the global means for each answer variable; τ_i is the factor A, corresponding to start type; β_j is the factor B concerning to the CA/GA ratio; $(\tau\beta)_{ij}$ corresponds to the interaction between factors A and B; and ε_{ijn} is the error [40]. The analysis of variance (ANOVA) was carried out using the Statgraphics Centurion XIX software, with a confidence level of 95% ($p > 0.05$), which ensures sound and consistent results [40]. The effect of each factor and the interaction between them on each answer variable were analyzed.

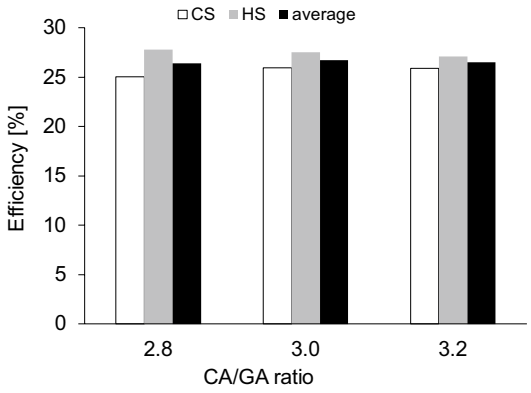

Fig. 4 Energy efficiency of the biomass gasification-based cookstove as a function of the CA/GA ratio and start type under the modified WBT version 4.2.3

3 Results and discussion

3.1 Energy and environment performance of the cookstove

Although the start types and the CA/GA ratio had no statistical significance (p value > 0.05) on the answer variables η (%), SE_{CO} (g/MJ_d), SE_{NO} (g/MJ_d), SE_{NO2} (g/MJ_d), nor SE_{TSPM} (mg/MJ_d), the trends of the results found here are analyzed and contrasted with the values reported in the scientific literature. This was done in order to compare the results and the improvements attained in energy efficiency and pollutant emissions as opposed to traditional stoves, as well as analyzing the phenomenology linked to the trends found as a function of the air flows ratio and the start type. The p-value obtained for each answer variable is shown in Table 1. The experimental results of the gasification-based cookstove are shown in Figs. 4, 5, and 6, which were drawn using Excel.

Table 1 p value for each answer variable

Factor	Efficiency (%)	NO_2 (g/MJ_d)	NO (g/MJ_d)	TSPM (mg/MJ_d)	CO (g/MJ_d)
CA/GA	0.7795	0.5022	0.7721	0.8895	0.7313
Start type	0.0949	0.0681	0.4133	0.1912	0.2137
Interaction	0.7964	0.3291	0.6806	0.4697	0.5871

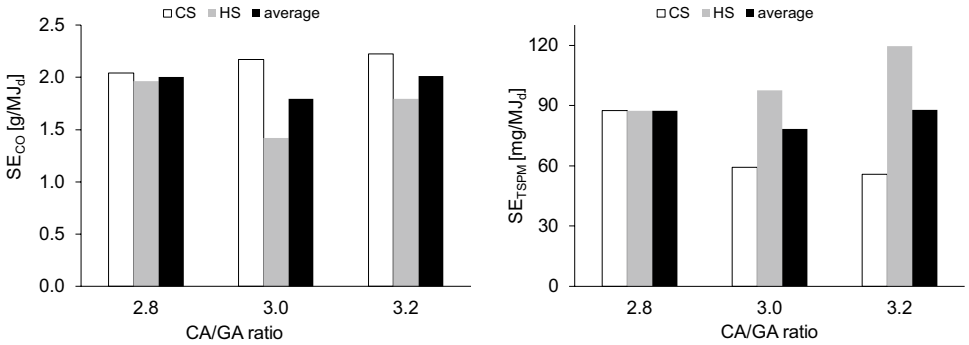

(a) CO specific emissions (b) TSPM specific emissions

Fig. 5 Specific CO and TSPM emissions from the gasification-based cookstove as a function of the CA/GA ratio and start type under the modified WBT version 4.2.3

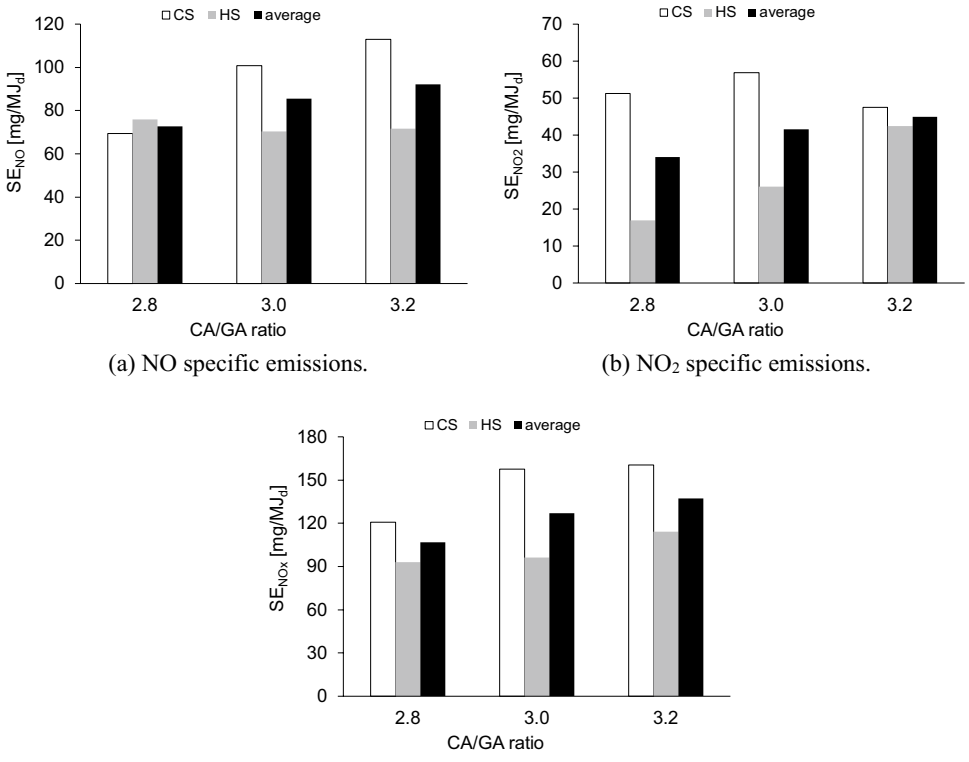

(a) NO specific emissions. (b) NO_2 specific emissions.

(c) NO_x specific emissions.

Fig. 6 NO, NO_2, and NO_x specific emissions from the gasification-based cookstove as a function of the CA/GA ratio and start type under the modified WBT version 4.2.3

The experimental factor CA/GA ratio does not have a statistically significant effect on the energy and emissions parameters studied here. This behavior is ascribed to a variation lower than 6% of the Reynolds number of the CA through the combustion chamber. Therefore, the constant gasification air (GA = 146 L/min) supplied for all experimental modes as well as the combustion air supplied for the CA/GA ratios of 2.8, 3.0, and 3.2 (CA = 408.8 L/min, 438.0 L/min, and 467.2 L/min, respectively) favored similar airflow conditions, which led to find not statistical significant variations of the answer variables (η, SE_{CO}, SE_{NO}, SE_{NO2}, and SE_{TSPM}) as a function of the CA/GA ratio.

3.2 Energy efficiency

In Fig. 4, the energy efficiency results of the cookstove are presented as a function of the start type. The average efficiency was 25.63% for the cold start (CS), while for the hot start (HS), the efficiency was 27.48%, representing an increase of ~ 7% when moving from CS to HS. The higher efficiency reached for the HS is ascribed to the remaining heat in the cookstove body, which favored higher temperatures during the gasification process. Consequently, the gasification reactions were activated (Boudouard reaction, dehydrogenation, water–gas reaction, steam reforming, and

carbonization) [41]. These reactions promote a higher yield of fuel gases (CO, H_2, and CH_4), which are oxidized by the air injected in the combustion zone (denoted combustion-air) and increase the energy released in the cookstove for boiling the water. Furthermore, the increment in the producer gas low heating value, during the HS, favored that the CGE increased by 8% regarding that of CS (Table 2); consequently, the producer gas thermal power also increases under the hot start mode. Therefore, the thermal efficiency of the cookstove increases due to the higher concentration of fuel gases and their high heat release rate (see Table 2) [42, 43]. Other authors have reported similar trends, Carter et al. [14] found thermal efficiencies for the cold start between 26 and 27%, while for the hot start the efficiency ranged between 32 and 33%. The cookstove behavior was reached using the waste of pine trees as fuel with a moisture content of 5.84%. Quist et al. [44] reported that the thermal efficiency of an improved gasification cookstove ranged from 11.3% to 16.5% for the cold start and from 16.3 to 18.5% for the hot start, using unprocessed wood as fuel. Sonarkar et al. [17] characterized a gasification cookstove and found an efficiency of 26% for the cold start and 27% for the hot start under the WBT protocol, working with wood pellets as fuel. The packing factor of pellets is high due to its bulk density (Sect. 2.1), which causes that the radiative heat transfer penetration in the solid phase diminishes [45], and in consequence, the biomass consumption rate diminishes, while the biochar yield increases [46, 47]. Hence, the energy supplied by the biomass to boil the water diminishes (denominator of Eq. (1)), whereby the thermal efficiency of the cookstove increases (Eq. (1)).

Figure 4 shows the average efficiency of the gasification-based cookstove (average value of CS and HS, -average-) as a function of the CA/GA ratio. The cookstove reaches the maximum efficiency at CA/GA = 3.0 ($\eta = 26.74\%$), which is attributed to a better mixture of combustion air with the ascending stream of the producer gas, promoting a suitable fuel gas oxidation; therefore, the heat release rate increases.

Table 2 Parameters of gasification-based cookstove as a function of the start type (cold and hot)

Gasification parameters	Start type	
	CS	HS
Producer gas composition (*vol%*)		
CO	10.98	13.31
CH_4	2.48	3.17
H_2	5.39	5.74
C_3H_8	0.08	0.11
LHV_{pg} (MJ/Nm^3)	2.93	3.53
CGE (%)	54.25	58.61
Y_{char} (wt%)	11.87	12.49

A suitable mixture between the combustion air and the producer gas favors a combustion efficiency improvement, and consequently, a high thermal efficiency of the gasification-based cookstove [16, 48]. Nevertheless, the thermal efficiency tends to diminish at CA/GA ratios higher than 3.2. If combustion-air flow increases, the homogeneous combustion zone (flame front) can be cooled, which reduces the combustion temperature and the convective heat transfer toward the pot. Therefore, the cookstove efficiency decreases [16, 49]. It is worth note that combustion air velocities used here are suitable because the combustion flame of the producer gas was not extinguished during the experimental campaign. Caubel et al. [50] reported a reduction in the thermal efficiency from 27 to 24% by increasing the volumetric flow of secondary air from 21 L/min to 35 L/min. The fuel used was unprocessed wood. Deng et al. [51] concluded that a total air injection (92 L/min) does not supply enough air for a complete oxidation of the gaseous fuel derived from wood pellets gasification. Additionally, an excess in the total air intake (276 L/min) may promote a slight fuel gas retention inside the combustion zone, thus affecting the thermal efficiency of the cookstove.

The values found in this study for the energy efficiency of the forced-draft gasification-based cookstove are comparable to other advanced technologies (rocket stove, Phillips stove, gasifier cookstove, and others) applied into cooking and based on biomass gasification, whose reported efficiencies reached values between 22 and 45% [17, 52–54]. Furthermore, it is highlighted that the efficiency of the gasification-based biomass cookstove analyzed here, for CA/GA = 3.0, was 91% higher than the efficiency of traditional three-stone cookfires that achieved efficiencies up to ~ 14% [2, 55, 56]. The thermal efficiency is affected by the controllable process parameters associated with the cookstoves. Furthermore, the design conditions (such as refractory walls and combustion chamber design) and the performance parameters (the energy released by the fuel and the energy delivered to the pot) directly influence the stoves' thermal efficiency.

3.3 Pollutant emissions

3.3.1 *Specific emissions of carbon monoxide (SECO, g/MJ$_d$)*

Figure 5a shows the specific emissions of carbon monoxide (SE_{CO}) as a function of the start type and CA/GA ratio. The average emissions for SE_{CO} were 2.15 g/MJ$_d$ and 2.12 g/MJ$_d$ during CS and HS, respectively. This slight reduction of ~ 2% when moving from CS to HS is a consequence of the cookstove preheating when working under HS. With the preheated cookstove (HS), higher temperatures are reached (~ 690 K) and, thus, the reactivity and oxidation of the fuel gas are favored [48]; consequently,

CO emissions decrease by 0.03 g/MJ_d. The higher concentration of CO and CH_4 in the producer gas, under HS (see Table 2), favors the temperature increment in the oxidation stage of the producer gas (combustion chamber). This temperature increment is ascribed to the increase of the producer gas heating value as well as of the heat release during its combustion [16]. On the other hand, under the CS stage, the CO-specific emissions increased by 8.5% as CA/GA ratio rose from 2.8 to 3.2. This CO increment was ascribed to the cooling effect that causes the high amount of combustion air supplied on the flame of the producer gas. Hence, the reduction of the flame temperature and the cookstove temperature (ambient temperature for CS) inhibit the oxidation reactions in the combustion chamber and, consequently, the CO-specific emissions tended to rise [57–60]. It is wort note that the specific CO emissions of our gasification-based cookstove diminished by ~ 86% (under cold and hot starts) regarding traditional three-stone cookstoves (15.50 g/MJ_d) [56]. The values found in this work are comparable with the specific CO emissions reported in the literature. Rapp et al.[61] reported specific CO emissions between 3 g/MJ_d and 7 g/MJ_d for gasification-based cookstoves evaluated under the WBT version 4.2.3; pine wood was used as fuel with a moisture content of 7%. Kshirsagar et al. [20] reported CO emissions of 2.14 g/MJ_d in a hybrid (natural and forced draft) gasification stove characterized under WBT 4.3.2, using wood as fuel with 10.37% moisture content.

The average CO-specific emissions (CS and HS average) as a function of the CA/GA ratio are also presented in Fig. 5a. For CA/GA = 3.0, a minimum value of SE_{CO} was reached (1.80 g/MJ_d), while in the extremes (CA/GA = 2.8 and 3.2), the CO specific emissions increased up to 2 g/MJ_d and 2.01 g/MJ_d, respectively. The CA/GA = 3.0 ratio favored a homogeneous distribution of the combustion-air through the combustion chamber. Consequently, the combustion efficiency of the producer gas increased [62] and so the SE_{CO} diminished by 0.2 g/MJ_d. These results meet the combustion theory, where both the defect and the excess of the air may cause the increase of CO-specific emissions [49]. A low CA/GA ratio means that a lower amount of secondary air is fed, which favors incomplete oxidation of the producer gas and, thus, increases CO emissions. Meanwhile, a greater amount of combustion air supplied (CA/GA = 3.2) may lead to reduce the temperature in the combustion zone, mitigating the gasification gas reactivity and, thus, increasing emissions [63]. Kirch et al. [64] characterized a TLUD stove using pine chips as fuel and reported volumetric flows of combustion air (~ 328 L/min) that did not provide enough oxygen for complete oxidation of the gas fuel; however, a limit of the combustion airflow (492 L/min) to avoid the cooling and extinguishing of the flame front was reported.

3.3.2 *TSPM specific emissions (SETSPM, mg/MJ_d)*

Figure 5b shows the specific emissions of the total suspended particle matter (SE_{TSPM}) as a function of the start type. For CS, an average emission of 67.50 mg/MJ_d was reached, while for HS, the average emissions increased up to 101.45 mg/MJ_d. This means that SE_{TSPM} increases by ~ 50% when the start types change from CS to HS. For the WBT test under HS, a more intense pyrolysis front is developed due to the higher temperature (~ 690 K) of the thermochemical conversion process (gasification), favoring tar formation. Tars are precursors of particle matter production by mechanisms of reaction such as dehydrogenation and carbonization, which occur at a temperature of ~ 650 K [65]. Concerning the TSPM emissions for CS as a function of the CA/GA ratio, SE_{TSPM} follows a trend opposite to that of HS (Fig. 5b). For CS, the producer gas composition reached a lower tar concentration; C_3H_8 decreased by 27.27% when compared to the HS (Table 2). This reduction was a consequence of the lower gasification temperature reached in the process because the cookstove was not preheated (cold start). Therefore, the low tar concentration contributed to inhibit the particle matter formation and, as a consequence, their emissions decreased [66]. Comparing the specific emissions of TSPM between the reported traditional three-stone cookstoves, 219 mg/MJ_d and 347 mg/MJ_d [67, 68], and the emissions achieved by the gasification-based cookstove assessed here, it is highlighted that the improved cookstove reduced the TSPM emissions between 69 and 81%. The specific emissions of TSPM released by the TLUD cookstove are comparable and even lower than that those reported in the literature (reduction in emission of TSPM > 50% in contrast with other improved stoves to be shown next). Osei et al. [69] reported emissions of TSPM of about 932.73 mg/MJ_d from a reverse-downdraft gasifier analyzed through the WBT protocol using rice husk as fuel. Boafo et al. [70] reported TSPM emissions between 220 mg/MJ_d and 430 mg/MJ_d for gasification-based cookstoves characterized under WBT version 4.3.2, using charcoal produced from the Neem tree as fuel with a 9.3% moisture content.

Figure 5b shows the TSPM average emissions between CS and HS as a function of the CA/GA ratio. For CA/GA ratio = 3.0, the TSMP emissions reached a minimum value (78.32 mg/MJ_d), while the emissions of 87.37 mg/MJ_d and 87.72 mg/MJ_d correspond to CA/GA ratios of 2.8 and 3.2, respectively. This increment of ~ 12% in the average TSPM, when moving from CA/GA = 3.0 to CA/GA ratio = 2.8, is a direct consequence of the oxygen deficit present in the combustion area that promotes incomplete combustion and the soot formation [71]. On the other hand, when moving from CA/GA = 3.0 to CA/GA = 3.2, the ~ 12% increase in the TSPM is attributed to a lessening of the flame front, which affects the reactivity of the producer gas, promoting

the formation of solid particles [22, 72]. It is worth noting that for CA/GA = 2.8, the variation of TSMP emissions is mild since the combustion air supplied for this condition (202 L/min) is the lowest airflow tested. Therefore, the residence time of particle matter, carried by the producer gas, increases in the combustion chamber; therefore, the oxidation of particle matter is favored for both starts (cold and hot). Kshirsagar et al. [63] found an optimal emission factor of particle matter, 120 mg/MJ_d, associated with a proper relation between five controllable process parameters such as the relation between the intake area, the primary air and secondary air ratio, the separation of the pot, the surface/volume relation of the fuel, and the pot diameter. Lai et al.[73] concluded that the gasification-based cookstoves with primary air (gasification) and secondary air (combustion) control possibilities can achieve better combustion efficiency and low pollutant emissions of particle matter. Liu et al. [74] stated that the variability in CO emissions is highly related to the combustion efficiency, while the particle matter emissions are mainly affected by the biomass type and the cookstove model.

3.3.3 Specific emissions of nitrogen oxides NO_x (SE_{NO_x}, mg/MJ_d)

Figure 6a, b shows the NO and NO_2 specific emissions, respectively, as a function of the start type and the CA/GA ratio. For the CS, the average SE_{NO} was 94.35 mg/MJ_d, while the average SE_{NO2} was 51.94 mg/MJ_d. For the tests under HS, 72.62 mg/MJ_d was reached for SE_{NO} and 28.51 mg/MJ_d for $SE_{NO2,}$ as average specific emissions. When moving from CS to HS, NO, and NO_2 emissions attained a reduction of ~ 30% and ~ 45%, respectively. This reduction in NO_x emissions was attributed to the higher biomass-air equivalence ratio (F_{rg} = 1.59) reached during HS, which produces fuel-rich zones (biomass) inside the gasifier during the gasification process, and consequently, a higher fuel gas yield (see Table 2), which favors the conversion of devolatilization products (including NH_3 and NO_2) in N_2 due to the lean availability of O_2 in the gasifier, whereby the NO formation from volatile species is inhibited [75, 76].

One of the main precursors of NO formation is the NH_3 radical, which is formed at low reaction temperatures (between 200 and 400 °C). NH_3 is produced by the deamination reaction of unstable amine compounds and the decomposition of cellulose in biomass. Therefore, under CS, the NH_3 present in the producer gas reacts to produce NO [77–79], whereas, during HS, the temperatures of the gasification process are higher than 700 °C [80, 81]. Consequently, NH_3 formation is inhibited by the activation of CO due to the reaction: $NH_3 + CO \rightarrow HCN + H_2O$, which takes place in the temperature ranges between 700 and 900 °C [82]. Hence, NO emissions tend to decrease for HS and NO_x emissions are attributed to the N content in the fuel. Bhattu et al. [21] reported an increase of ~ 3.6 times in the SE_{NO_x} when changing the wood fuel to wheat pellets, which is attributed to the second fuel having a higher nitrogen content. Deng et al. [83] got average NO_x specific emissions of 20 mg/kg_{bms} using wood pellets in a forced-draft gasification-based cookstove. The NO_x released from the biomass gasification is related to the fuel because the biomass has a high N content, and the combustion/gasification temperature is usually lower than the temperatures that favor the thermal formation of NO_x (1300 °C) [84].

NO and NO_2 and their average values for CS and HS are shown in Fig. 6a, b. A trend to increase NO_x emissions with the CA/GA ratio is observed in both graphs. SE_{NO} went from 72.64 mg/MJ_d for CA/GA = 2.8 up to 92.28 mg/MJ_d for CA/GA = 3.2. Similarly, the SE_{NO2} ranged from 34.13 mg/MJ_d up to 45.01 mg/MJ_d for CA/GA = 2.8 and CA/GA = 3.2, respectively. Analogous trends to the ones found in this work were reported by Deng et al. [51], who analyzed the effect of the primary and secondary air injection on the NO_x emissions of a forced-draft gasification-based cookstove. NO_x emissions increase from 805 to 1041 mg by increasing the total airflow from 92 to 276 L/min. The increment of the combustion-air mass flow causes NO_x emissions to rise. Such increment is ascribed to the $HCN + NH_3$ radical reaction [85]. Therefore, it was worth noting that an excess in the total air injection may favor N of the fuel reaction with the oxygen to produce NO_x.

In this work, the NO_x average specific emissions for all operation modes of the gasification-based cookstove were 123.72 mg/MJ_d, whose value is attributed to the low biomass *N* content (*N*, 0.02 wt%), see Fig. 6c. The NO_x emissions measured are similar and even lower than those reported in the literature. Shrestha et al. [22] reported an average NO_x emission factor of 336 mg/MJ_d for nine improved Chinese cookstoves, using pear wood as fuel. These emissions were attributed to the amount of nitrogen in the fuel (~ 1.31 wt%). Ozgen et al. [84] reached NO_x emissions of ~ 76 mg/MJ from a home boiler used for heating, fed with lignocellulosic (walnut shell) biomass as fuel ($N < 0.4\%$wt). Kistler et al. [86] reported NO_x emissions between 58 mg/MJ and 132 mg/MJ for a biomass cookstove fed with different fuels. Finally, Fachinger et al. [87] found an average NO_x specific emission of 40 mg/MJ in a biomass-combustion advanced cookstove, using 11 hardwood species and 4 softwood species as fuel.

Thus, the NO_x specific emissions found in this work are attributed to the reaction mechanism of the N-biomass oxidation. The biomass gasification in this cookstove does not reach temperatures (> 1300 °C) that promote NO_x thermal formation by atmospheric nitrogen oxidation [84, 88]. Therefore, the NO_x formation in the cookstove is not favored due to a high gasification equivalence ratio (F_{rg} = 1.59), which allows to reach fuel-rich zones (biomass-air), and

consequently, the NO_x reduction in N_2 is favored due to the limited availability of O_2 in the gasification process, which inhibits the NO formation from volatile species [75, 89].

Concerning the producer gas oxidation in the combustion chamber, the adiabatic flame temperature of the producer gas has been calculated based on the first law of thermodynamics applied to reactive systems [90] and is shown in Fig. 7. The calculi were carried out using the Engineering Equation Solver software (EES) by varying the CA/GA ratio between 2.0 and 4.0. The adiabatic flame temperature decreases if the combustion air increases. This is a consequence of the cooling of the reaction zone (combustion chamber) caused by the excess combustion air supplied (see Fig. 7). Therefore, according to Fig. 7, under HS conditions, the producer gas adiabatic flame temperature is higher than that of CS (> 200 °C). Nevertheless, the adiabatic flame temperature decreases if CA/GA ratio increases; this behavior is caused by the excess of combustion air, which leads to decrease the flame temperature because a high amount of flue gases is heated by the same mass of the producer gas. Therefore, based on the maximum adiabatic flame temperature of the producer gas (~1000 °C), it is highlighted that the trends of the NO_x emissions from the TLUD cookstove analyzed here could be attributed to the N-biomass activation [36, 91, 92].

The reduction of the NO_x specific emissions contributes to the improvement of the indoor air quality because prolonged exposure to this gaseous pollutant irritates the respiratory system and, in some cases, may promote the onset of chronic respiratory diseases. NO_x is a precursor in forming ground-level ozone (O_3), which is the main component of smog. Besides, when NO_x reacts with ammonia (NH_3) present in the atmosphere, it becomes the main contributing factor in secondary soot formation ($PM_{2.5}$) [93]. Prolonged exposition to high concentrations of O_3 and $PM_{2.5}$ brings about respiratory problems, such as asthma and pneumonia, bronchitis, and lung capacity reduction [5, 87]. The NO_x is the main forming agents of N_2O, which is an important greenhouse gas. Furthermore, N_2O promotes soil acidification, lake, and river eutrophication, and consequently, the biologic biodiversity is adversely affected [5].

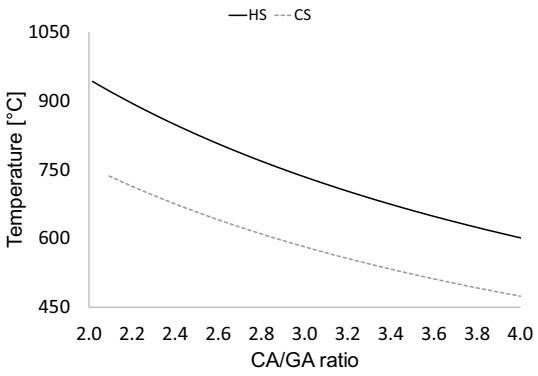

Fig. 7 Adiabatic flame temperature of the producer gas as a function of the start type and the CA/GA ratio of the gasification-based cookstove

3.4 Energy characterization of the gasification process

The thermodynamic characterization of the gasification process was assessed as a function of the start type (CS, HS) of the WBT protocol. Table 2 shows the answer variables of the gasification process, such as the composition and low heating value (LHV_{pg}) of the producer gas, the cold gas efficiency (CGE), and the biochar yield (Y_{char}). From CS to HS, an increase in the concentration of gaseous fuels such as CO (~22%), CH_4 (~28%), and H_2 (~7%) was observed. The higher concentration of fuel gases for HS is attributed to the fact that gasification reactions (Boudouard reaction, dehydrogenation, water–gas reaction, steam reforming, and carbonization) were favored by the preheating induced in the cookstove [94, 95]. Consequently, LHV_{pg} increases due to the higher volumetric concentration of the gaseous fuels (CO, CH_4, and H_2) [96]. LHV_{pg} went from 2.93 MJ/Nm^3 under CS condition up to 3.53 MJ/Nm^3 for HS. Therefore, the cold gas efficiency (CGE) increased from 54.25% in the CS condition up to 58.61% under HS. Therefore, the CGE increment is attributed to the increase of the LVH_{pg} because the energy supplied by the biomass is constant.

The char yield increased by ~ 5% when going from 11.87% in the CS condition up to 12.49% under HS. The intensification of the pyro-combustion front promoted by the higher temperatures reached under HS mode allows to increase the LHV_{pg}. The high energy content of the gaseous fuel contributes to reducing the cooking time in the cookstove, and in consequence, the biochar yield increases. Thus, it is highlighted that the biochar yield rises under HS conditions due to the inverse relationship between the biochar yield and the cooking time [97].

4 Conclusions

In this work, an optimal air flow ratio (CA/GA = 3.0) was found because it favored the highest thermal efficiency of the gasification-based cookstove (~26.74%). The homogeneous mixture between the combustion-air and the producer gas fostered a suitable oxidation of the gaseous fuel. Consequently, the heat release rate to the pot increased.

The specific emissions of CO and TSPM reached minimum values for CA/GA = 3.0, 1.8 g/MJ_d, and 78.32 mg/MJ_d, respectively. The minimum emissions of CO are ascribed to the suitable combustion air supply that favored the producer gas oxidation promoting the transformation of CO into CO_2.

However, NO_x emissions tend to rise with the combustion air injection (for both conditions, CS and HS). The nitrogen activation present in the fuel is attributed to its reaction with the O_2 excess (CA/GA > 3.0) since the requirements for the thermal formation of NO_x, associated with reaction temperatures higher than 1300 °C, were not achieved in the TLUD cookstove.

The gasification process reached a better energy behavior during hot start condition, which is attributed to the cookstove preheating. The remaining heat in the cookstove body favored the gasification stages. Consequently, CO, H_2, and CH_4 concentrations increased, improving the LHV_{pg} by ~ 20%, which leads to increase CGE and Y_{char} by ~ 8% and 5%, respectively. Therefore, the thermal efficiency of the gasification-based cookstove increased by ~ 7%.

Acknowledgements The authors acknowledge the financial support of the Sistema General de Regalías (SGR) from Colombia through the research project (BPIN 2020000100500) PRG2022-51570. And the support of the University of Antioquia is also acknowledged through the young researcher program (*Programa de Joven Investigador*), as well as the funding for the undergraduate thesis (code PR21-1-08).

Funding Open Access funding provided by Colombia Consortium.

Declarations

Conflict of interest The authors declare that there is not any type of conflict-of-interest relationship with this investigation.

References

1. Pundle A, Sullivan B, Means P, Posner JD, Kramlich JC (2019) Predicting and analyzing the performance of biomass-burning natural draft rocket cookstoves using computational fluid dynamics. Biomass Bioenergy 131:105402. https://doi.org/10.1016/j.biombioe.2019.105402
2. Gupta A, Mulukutla ANV, Gautam S, TaneKhan W, Waghmare SS, Labhasetwar NK (2020) Development of a practical evaluation approach of a typical biomass cookstove. Environ Technol Innov 17:100613. https://doi.org/10.1016/j.eti.2020.100613
3. Rasoulkhani M, Ebrahimi-Nik M, Abbaspour-Fard MH, Rohani A (2018) Comparative evaluation of the performance of an improved biomass cook stove and the traditional stoves of Iran. Sustain Environ Res 28:438–443. https://doi.org/10.1016/j.serj.2018.08.001
4. WHO Global Air Quality Guidelines Working Group on Risk of Bias Assessment (2020) Risk of bias assessment instrument for systematic reviews informing who global air quality guidelines By: the WHO Global Air Quality Guidelines Working Group on Risk of Bias Assessment. http://apps.who.int/bookorders.
5. Bray CD, Battye WH, Aneja VP, Schlesinger WH (2021) Global emissions of NH_3, NO_x, and N_2O from biomass burning and the impact of climate change. J Air Waste Manag Assoc 71:102–114. https://doi.org/10.1080/10962247.2020.1842822
6. Hodan WM, Barnard WR (2004) Evaluating the contribution of PM2.5 precursor gases and re-entrained road emissions to mobile source PM2.5 particulate matter emissions. MACTEC Under Contract to the Federal Highway Administration. https://www3.epa.gov/ttnchie1/conference/ei13/mobile/hodan.pdf.
7. Otero N, Rust HW, Butler T (2021) Temperature dependence of tropospheric ozone under NOx reductions over Germany. Atmos Environ 253:118334. https://doi.org/10.1016/j.atmosenv.2021.118334
8. Toro MV, Cremades LV, Calbó J (2006) Relationship between VOC and NOx emissions and chemical production of tropospheric ozone in the Aburrá Valley (Colombia). Chemosphere 65:881–888. https://doi.org/10.1016/j.chemosphere.2006.03.013
9. Consorcio Estrategia Rural Sostenibles (2019) Realizar un estudio que permita formular un programa actualizado de sustitución progresiva de leña como energético en el sector residencial de Colombia, con los componentes necesarios para su ejecución 355. https://www1.upme.gov.co/Hidrocarburos/Plan_sustitucion_progresiva_Lena.pdf.
10. D. Aguiar-Gil, L.M. Gómez-Peláez, T. Álvarez-Jaramillo, M.A. Correa-Ochoa, J.C. Saldarriaga-Molina, Evaluating the impact of PM2.5 atmospheric pollution on population mortality in an urbanized valley in the American tropics, Atmos Environ. 224 (2020). https://doi.org/10.1016/j.atmosenv.2020.117343.
11. Olsen Y, Nøjgaard JK, Olesen HR, Brandt J, Sigsgaard T, Pryor SC, Ancelet T, del Viana M, Querol X, Hertel O (2020) Emissions and source allocation of carbonaceous air pollutants from wood stoves in developed countries: a review. Atmos Pollut Res 11:234–251. https://doi.org/10.1016/j.apr.2019.10.007
12. Suresh R, Singh VK, Malik JK, Datta A, Pal RC (2016) Evaluation of the performance of improved biomass cooking stoves with different solid biomass fuel types. Biomass Bioenergy 95:27–34. https://doi.org/10.1016/j.biombioe.2016.08.002
13. Jetter J, Zhao Y, Smith KR, Khan B, Yelverton T, Decarlo P, Hays MD (2012) Pollutant emissions and energy efficiency under controlled conditions for household biomass cookstoves and implications for metrics useful in setting international test standards. Environ Sci Technol 46:10827–10834. https://doi.org/10.1021/es301693f
14. Carter EM, Shan M, Yang X, Li J, Baumgartner J (2014) Pollutant emissions and energy efficiency of chinese gasifier cooking stoves and implications for future intervention studies. Environ Sci Technol 48:6461–6467. https://doi.org/10.1021/es405723w
15. Kirch T, Medwell PR, Birzer CH (2016) Natural draft and forced primary air combustion properties of a top-lit up-draft research furnace. Biomass Bioenergy 91:108–115. https://doi.org/10.1016/j.biombioe.2016.05.003
16. Caubel JJ, Rapp VH, Chen SS, Gadgil AJ (2020) Practical design considerations for secondary air injection in wood-burning cookstoves: An experimental study. Dev Eng 5:100049. https://doi.org/10.1016/j.deveng.2020.100049
17. Sonarkar PR, Chaurasia AS (2019) Thermal performance of three improved biomass-fired cookstoves using fuel wood, wood pellets and coconut shell. Environ Dev Sustain 21:1429–1449. https://doi.org/10.1007/s10668-018-0096-0

18. Tryner J, Tillotson JW, Baumgardner ME, Mohr JT, DeFoort MW, Marchese AJ (2016) The effects of air flow rates, secondary air inlet geometry, fuel type, and operating mode on the performance of gasifier cookstoves. Environ Sci Technol 50:9754–9763. https://doi.org/10.1021/acs.est.6b00440
19. Mehta Y, Richards C (2017) Gasification performance of a top-lit updraft cook stove. Energies (Basel). https://doi.org/10.3390/en10101529
20. Kshirsagar MP, Kalamkar VR (2020) Application of multi-response robust parameter design for performance optimization of a hybrid draft biomass cook stove. Renew Energy 153:1127–1139. https://doi.org/10.1016/j.renene.2020.02.049
21. Bhattu D, Zotter P, Zhou J, Stefenelli G, Klein F, Bertrand A, Temime-Roussel B, Marchand N, Slowik JG, Baltensperger U, Prévôt ASH, Nussbaumer T, El Haddad I, Dommen J (2019) Effect of stove technology and combustion conditions on gas and particulate emissions from residential biomass combustion. Environ Sci Technol 53:2209–2219. https://doi.org/10.1021/acs.est.8b05020
22. Shrestha P, Zhang W, Mawusi SK, Li J, Xu J, Li C, Xue C, Liu G (2021) In-use emissions and usage trend of pellet heating stoves in rural Yangxin, Shandong Province. Environ Pollut 280:116955. https://doi.org/10.1016/j.envpol.2021.116955
23. Scharler R, Archan G, Rakos C, von Berg L, Lello D, Hochenauer C, Anca-Couce A (2021) Emission minimization of a top-lit updraft gasifier cookstove based on experiments and detailed CFD analyses. Energy Convers Manag. https://doi.org/10.1016/j.enconman.2021.114755
24. Lenis YA, Pérez JF (2014) Gasification of sawdust and wood chips in a fixed bed under autothermal and stable conditions. Energy Sources Part A: Recov Util Environ Effects. https://doi.org/10.1080/15567036.2013.875081
25. Díez HE, Gómez IN, Pérez JF (2018) Mass, energy, and exergy analysis of the microgasification process in a top-lit updraft reactor: effects of firewood type and forced primary airflow. Sustain Energy Technol Assess 29:82–91. https://doi.org/10.1016/j.seta.2018.07.003
26. Sutar KB, Kohli S, Ravi MR, Ray A (2015) Biomass cookstoves: a review of technical aspects. Renew Sustain Energy Rev 41:1128–1166. https://doi.org/10.1016/j.rser.2014.09.003
27. PCIA & Global Alliance (2013) The Water Boiling Test Version 4.2.3; Cookstove emissions and efficiency in a controlled laboratory setting. Global Alliances Clearn Cookstoves 2:52
28. Gutiérrez J, Chica E, Pérez JF (2022) Parametric analysis of a gasification-based cookstove as a function of biomass density, gasification behavior, airflows ratio, and design. ACS Omega 7(9):7481–7498. https://doi.org/10.1021/acsomega.1c05137
29. Jetter JJ, Kariher P (2009) Solid-fuel household cook stoves: Characterization of performance and emissions. Biomass Bioenergy 33:294–305. https://doi.org/10.1016/j.biombioe.2008.05.014
30. Arora P, Jain S, Sachdeva K (2014) Laboratory based assessment of cookstove performance using energy and emission parameters for North Indian cooking cycle. Biomass Bioenergy 69:211–221. https://doi.org/10.1016/j.biombioe.2014.07.012
31. Jain T, Sheth PN (2019) Design of energy utilization test for a biomass cook stove: formulation of an optimum air flow recipe. Energy 166:1097–1105. https://doi.org/10.1016/j.energy.2018.10.180
32. Hailu A (2022) Development and performance analysis of top lit updraft: natural draft gasifier stoves with various feed stocks. Heliyon 8:e10163. https://doi.org/10.1016/j.heliyon.2022.e10163
33. Soares Neto TG, Carvalho JA, Cortez EV, Azevedo RG, Oliveira RA, Fidalgo WRR, Santos JC (2011) Laboratory evaluation of Amazon forest biomass burning emissions. Atmos Environ 45:7455–7461. https://doi.org/10.1016/j.atmosenv.2011.05.003
34. Arora P, Das P, Jain S, Kishore VVN (2014) A laboratory based comparative study of Indian biomass cookstove testing protocol and Water Boiling Test. Energy Sustain Dev 21:81–88. https://doi.org/10.1016/J.ESD.2014.06.001
35. Huangfu Y, Li H, Chen X, Xue C, Chen C, Liu G (2014) Effects of moisture content in fuel on thermal performance and emission of biomass semi-gasified cookstove. Energy Sustain Dev 21:60–65. https://doi.org/10.1016/j.esd.2014.05.007
36. Patel S, Leavey A, He S, Fang J, O'Malley K, Biswas P (2016) Characterization of gaseous and particulate pollutants from gasification-based improved cookstoves. Energy Sustain Dev 32:130–139. https://doi.org/10.1016/j.esd.2016.02.005
37. Zhao J, Shi L, Duan W, Li H, Yi P, Tao W, Shen G, Tao S, Pan B, Xing B (2021) Emission factors of environmentally persistent free radicals in PM25 from rural residential solid fuels combusted in a traditional stove. Sci Total Environ 773:145151. https://doi.org/10.1016/j.scitotenv.2021.145151
38. González WA, Zimmermann F, Pérez JF (2019) Thermodynamic assessment of the fixed-bed downdraft gasification process of fallen leaves pelletized with glycerol as binder. Case Stud Therm Eng 14:100480. https://doi.org/10.1016/j.csite.2019.100480
39. Guo F, Dong Y, Dong L, Guo C (2014) Effect of design and operating parameters on the gasification process of biomass in a downdraft fixed bed: an experimental study. Int J Hydrogen Energy 39:5625–5633. https://doi.org/10.1016/j.ijhydene.2014.01.130
40. Jensen WA (2014) Design and analysis of experiments by douglas montgomery: a supplement for using JMP®. J Qual Technol 46:181–181. https://doi.org/10.1080/00224065.2014.11917962
41. Maneerung T, Li X, Li C, Dai Y, Wang CH (2018) Integrated downdraft gasification with power generation system and gasification bottom ash reutilization for clean waste-to-energy and resource recovery system. J Clean Prod 188:69–79. https://doi.org/10.1016/j.jclepro.2018.03.287
42. James AMR, Yuan W, Wang D, Wang D, Kumar A (2020) The effect of gasification conditions on the surface properties of biochar produced in a top-lit updraft gasifier. Appl Sci (Switzerland) 10:11–13. https://doi.org/10.3390/app10020688
43. Mehta Y, Richards C (2020) Effect of air flow rate and secondary air jets on the operation of TLUD gasifier cookstove. Int J Sustain Energ 39:207–217. https://doi.org/10.1080/14786451.2019.1671388
44. Quist CM, Jones MR, Lewis RS (2016) Estimation of transient thermal efficiency of a biomass cookstove. Energy Sustain Dev 33:122–128. https://doi.org/10.1016/j.esd.2016.06.004
45. Kirch T, Medwell PR, Birzer CH, van Eyk PJ (2020) Small-scale autothermal thermochemical conversion of multiple solid biomass feedstock. Renew Energy 149:1261–1270. https://doi.org/10.1016/j.renene.2019.10.120
46. Lenis YA, Pérez JF, Melgar A (2016) Fixed bed gasification of Jacaranda Copaia wood: effect of packing factor and oxygen enriched air. Ind Crops Prod 84:166–175. https://doi.org/10.1016/j.indcrop.2016.01.053
47. González WA, Pérez JF, Chapela S, Porteiro J (2018) Numerical analysis of wood biomass packing factor in a fixed-bed gasification process. Renew Energy 121:579–589. https://doi.org/10.1016/j.renene.2018.01.057
48. Bentson S, Evitt D, Still D, Lieberman D, MacCarty N (2022) Retrofitting stoves with forced jets of primary air improves speed, emissions, and efficiency: evidence from six types of biomass cookstoves. Energy Sustain Dev 71:104–117. https://doi.org/10.1016/j.esd.2022.09.013
49. Kirch T, Birzer CH, Medwell PR, Holden L (2018) The role of primary and secondary air on wood combustion in cookstoves. Int

J Sustain Energ 37:268–277. https://doi.org/10.1080/14786451.2016.1166110
50. Caubel JJ, Rapp VH, Chen SS, Gadgil AJ (2018) Optimization of secondary air injection in a wood-burning cookstove: an experimental study. Environ Sci Technol 52:4449–4456. https://doi.org/10.1021/acs.est.7b05277
51. Deng M, Li P, Shan M, Yang X (2020) Optimizing supply air fl ow and its distribution between primary and secondary air in a forced-draft biomass pellet stove. Environ Res 184:109301. https://doi.org/10.1016/j.envres.2020.109301
52. Sharma M, Dasappa S (2017) Emission reduction potentials of improved cookstoves and their issues in adoption: an Indian outlook. J Environ Manag 204:442–453. https://doi.org/10.1016/j.jenvman.2017.09.018
53. Raman P, Murali J, Sakthivadivel D, Vigneswaran VS (2013) Performance evaluation of three types of forced draft cook stoves using fuel wood and coconut shell. Biomass Bioenergy 49:333–340. https://doi.org/10.1016/j.biombioe.2012.12.028
54. Samal C, Mishra PC, Mukherjee S, Das D (2019) Evolution of high performance and low emission biomass cookstoves—an overview. AIP Conf Proc 2200. https://doi.org/10.1063/1.5141191
55. Chica E, Pérez JF (2019) Development and performance evaluation of an improved biomass cookstove for isolated communities from developing countries. Case Stud Therm Eng 14:100435. https://doi.org/10.1016/j.csite.2019.100435
56. United NationsFoundation, Clean Cook Catalog (2021) http://catalog.cleancookstoves.org/pages/about. Accessed 1 Mar 2023
57. Himanshu, Kurmi OP, Jain S, Tyagi SK (2022) Performance assessment of an improved gasifier stove using biomass pellets: an experimental and numerical investigation. Sustain Energy Technol Assess 53:102432. https://doi.org/10.1016/j.seta.2022.102432
58. Parsons S, Tanner K, Champion W, Grieshop A (2022) The effects of modified operation on emissions from a pellet-fed, forced-draft gasifier stove. Energy Sustain Dev 70:259–271. https://doi.org/10.1016/j.esd.2022.08.004
59. Roden CA, Bond TC, Conway S, Osorto Pinel AB, MacCarty N, Still D (2009) Laboratory and field investigations of particulate and carbon monoxide emissions from traditional and improved cookstoves. Atmos Environ 43:1170–1181. https://doi.org/10.1016/j.atmosenv.2008.05.041
60. Barbour M, Udesen D, Bentson S, Pundle A, Tackman C, Evitt D, Means P, Scott P, Still D, Kramlich J, Posner JD, Lieberman D (2021) Development of wood-burning rocket cookstove with forced air-injection. Energy Sustain Dev 65:12–24. https://doi.org/10.1016/j.esd.2021.09.003
61. Rapp VH, Caubel JJ, Wilson DL, Gadgil AJ (2016) Reducing ultrafine particle emissions using air injection in wood-burning cookstoves. Environ Sci Technol 50:8368–8374. https://doi.org/10.1021/acs.est.6b01333
62. Himanshu, Pal K, Jain S, Tyagi SK (2022) Energy and exergy analysis and emission reduction from forced draft gasifier cookstove models: a comparative study. J Therm Anal Calorim 147:8509–8521. https://doi.org/10.1007/s10973-021-11137-y
63. Kshirsagar MP, Kalamkar VR, Pande RR (2020) Multi-response robust design optimization of natural draft biomass cook stove using response surface methodology and desirability function. Biomass Bioenergy 135:105507. https://doi.org/10.1016/j.biombioe.2020.105507
64. Kirch T, Birzer CH, Van Eyk PJ, Medwell PR (2018) Influence of primary and secondary air supply on gaseous emissions from a small-scale staged solid biomass fuel combustor. Energy Fuels 32:4212–4220. https://doi.org/10.1021/acs.energyfuels.7b03152
65. Hu Z, Peng Y, Sun F, Chen S, Zhou Y (2021) Thermodynamic equilibrium simulation on the synthesis gas composition in the context of underground coal gasification. Fuel 293:120462. https://doi.org/10.1016/j.fuel.2021.120462
66. Kang KT, Hwang JY, Chung SH, Lee W (1997) Soot zone structure and sooting limit in diffusion flames: comparison of counterflow and co-flow flames. Combust Flame 109:266–281
67. Mitchell EJS, Ting Y, Allan J, Lea-Langton AR, Spracklen DV, McFiggans G, Coe H, Routledge MN, Williams A, Jones JM (2020) Pollutant emissions from improved Cookstoves of the type used in Sub-Saharan Africa. Combust Sci Technol 192:1582–1602. https://doi.org/10.1080/00102202.2019.1614922
68. Arora P, Sharma D, Kumar P, Jain S (2020) Assessment of clean cooking technologies under different fuel use conditions in rural areas of Northern India. Chemosphere 257:127315. https://doi.org/10.1016/j.chemosphere.2020.127315
69. Osei I, Kemausuor F, Commeh MK, Akowuah JO, Owusu-Takyi L (2020) Design, Fabrication and Evaluation of Non-Continuous Inverted Downdraft Gasifier Stove Utilizing Rice husk as feedstock. Sci Afr 8:e00414. https://doi.org/10.1016/j.sciaf.2020.e00414
70. Boafo-Mensah G, Darkwa KM, Laryea G (2020) Effect of combustion chamber material on the performance of an improved biomass cookstove. Case Stud Therm Eng 21:100688. https://doi.org/10.1016/j.csite.2020.100688
71. Tryner J, Volckens J, Marchese AJ (2018) Effects of operational mode on particle size and number emissions from a biomass gasifier cookstove. Aerosol Sci Technol 52:87–97. https://doi.org/10.1080/02786826.2017.1380779
72. Kaur-Sidhu M, Ravindra K, Mor S, John S (2020) Emission factors and global warming potential of various solid biomass fuel-cook stove combinations. Atmos Pollut Res 11:252–260. https://doi.org/10.1016/j.apr.2019.10.009
73. Lai A, Shan M, Deng M, Carter E, Yang X, Baumgartner J, Schauer J (2019) Differences in chemical composition of PM2.5 emissions from traditional versus advanced combustion (semi-gasifier) solid fuel stoves. Chemosphere 233:852–861. https://doi.org/10.1016/j.chemosphere.2019.06.013
74. Liu X, Shen G, Chen L, Qian Z, Zhang N, Chen Y, Chen Y, Cao J, Cheng H, Du W, Li B, Li G, Li Y, Liang X, Liu M, Lu H, Luo Z, Ren Y, Zhang Y, Zhu D, Tao S (2021) Spatially resolved emission factors to reduce uncertainties in air pollutant emission estimates from the residential sector. Environ Sci Technol 55:4483–4493. https://doi.org/10.1021/acs.est.0c08568
75. Wang J, Lou HH, Yang F, Cheng F (2016) Development and performance evaluation of a clean-burning stove. J Clean Prod 134:447–455. https://doi.org/10.1016/j.jclepro.2016.01.068
76. Lee B-H, Sh L, Lee D-G, Jeon CH (2021) Effect of torrefaction and ashless process on combustion and NO_x emission behaviors of woody and herbaceous biomass. SSRN Electron J. https://doi.org/10.2139/ssrn.3706644
77. Zhan H, Zhuang X, Song Y, Yin X, Cao J, Shen Z, Wu C (2018) Step pyrolysis of N-rich industrial biowastes: regulatory mechanism of NOx precursor formation via exploring decisive reaction pathways. Chem Eng J 344:320–331. https://doi.org/10.1016/j.cej.2018.03.099
78. Xiao K, Yu Z, Wang H, Yang J, Liang S, Hu J, Hou H, Liu B (2019) Investigation on emission control of NOx precursors and phosphorus reclamation during pyrolysis of ferric sludge. Sci Total Environ 670:932–940. https://doi.org/10.1016/j.scitotenv.2019.03.223
79. Van Huynh C, Kong SC (2013) Combustion and NOx emissions of biomass-derived syngas under various gasification conditions utilizing oxygen-enriched-air and steam. Fuel 107:455–464. https://doi.org/10.1016/j.fuel.2012.12.016
80. Susastriawan AAP, Purwanto Y, Sidharta BW, Wahyu G, Trisna T, Setiawan RA (2021) Producer gas stove: design, fabrication,

and evaluation of thermal performance. J King Saud Univ Eng Sci. https://doi.org/10.1016/j.jksues.2021.10.009
81. Sutar KB, Kohli S, Ravi MR (2023) Clean cooking with downdraft biomass gasifier cookstove: effect of gasifier performance. Energy 263:125631. https://doi.org/10.1016/j.energy.2022.125631
82. Gao P, Guo D, Liang C, Liu G, Yang S (2020) Nitrogen conversion during the rapid pyrolysis of raw/torrefied wheat straw. Fuel 259:116227. https://doi.org/10.1016/j.fuel.2019.116227
83. Deng M, Li P, Shan M, Yang X (2019) Characterizing dynamic relationships between burning rate and pollutant emission rates in a forced-draft gasifier stove consuming biomass pellet fuels. Environ Pollut. https://doi.org/10.1016/j.envpol.2019.113338
84. Ozgen S, Cernuschi S, Caserini S (2021) An overview of nitrogen oxides emissions from biomass combustion for domestic heat production. Renew Sustain Energy Rev 135:110113. https://doi.org/10.1016/j.rser.2020.110113
85. Bugge M, Skreiberg Ø, Haugen NEL, Carlsson P, Seljeskog M (2015) Predicting NOx emissions from wood stoves using detailed chemistry and computational fluid dynamics. Energy Procedia 75:1740–1745. https://doi.org/10.1016/j.egypro.2015.07.446
86. Kistler M, Schmidl C, Padouvas E, Giebl H, Lohninger J, Ellinger R, Bauer H, Puxbaum H (2012) Odor, gaseous and PM10 emissions from small scale combustion of wood types indigenous to Central Europe. Atmos Environ 51:86–93. https://doi.org/10.1016/j.atmosenv.2012.01.044
87. Fachinger F, Drewnick F, Gieré R, Borrmann S (2017) How the user can influence particulate emissions from residential wood and pellet stoves: Emission factors for different fuels and burning conditions. Atmos Environ 158:216–226. https://doi.org/10.1016/j.atmosenv.2017.03.027
88. Shi W, Liu Y, He Y (2021) Analysis of air pollutant emission differences and emission reductions of coal-fired stoves of different residents. IOP Conf Ser Earth Environ Sci 632:052044. https://doi.org/10.1088/1755-1315/632/5/052044
89. Torres-Rojas D, Deng L, Shannon L, Fisher EM, Joseph S, Lehmann J (2019) Carbon and nitrogen emissions rates and heat transfer of an indirect pyrolysis biomass cookstove. Biomass Bioenergy 127:105279. https://doi.org/10.1016/j.biombioe.2019.105279
90. Y. a. Çengel, Thermodynamics: An Engineering Approach, McGraw-Hill. (2004).
91. Li N, Lu G, Li X, Yan Y (2016) Prediction of NOx emissions from a biomass fired combustion process based on flame radical imaging and deep learning techniques. Combust Sci Technol 188:233–246. https://doi.org/10.1080/00102202.2015.1102905
92. Zhang ZX, Sun ZF, Zhang YH, Ding HY, Zhou YG, Zhang YX, Riaz A, Crispin PP, Dong RJ (2017) Effects of biomass pellet composition on the thermal and emissions performances of a TLUD cooking stove. Int J Agric Biol Eng 10:189–197. https://doi.org/10.25165/j.ijabe.20171004.2963
93. Whalley et al (2021) Evaluating the sensitivity of radical chemistry and ozone formation to ambient VOCs and NOx in Beijing. Atmos Chem Phys 21:2125–2147. https://doi.org/10.5194/acp-21-2125-2021
94. Urych B, Smoliński A (2021) Sewage sludge and phytomass copyrolysis and the gasification of its chars: A kinetics and reaction mechanism study. Fuel. https://doi.org/10.1016/j.fuel.2020.119186
95. Hu Y, Cheng Q, Wang Y, Guo P, Wang Z, Liu H, Akbari A (2020) Investigation of biomass gasification potential in syngas production: characteristics of dried biomass gasification using steam as the gasification agent. Energy Fuels 34:1033–1040. https://doi.org/10.1021/acs.energyfuels.9b02701
96. Rabea K, Bakry AI, Khalil A, El-Fakharany MK, Kadous M (2021) Real-time performance investigation of a downdraft gasifier fueled by cotton stalks in a batch-mode operation. Fuel 300:120976. https://doi.org/10.1016/j.fuel.2021.120976
97. Birzer C, Medwell P, MacFarlane G, Read M, Wilkey J, Higgins M, West T (2014) A biochar-producing, dung-burning cookstove for humanitarian purposes. Procedia Eng 78:243–249. https://doi.org/10.1016/j.proeng.2014.07.063